Iron/multiwalled carbon nanotube (Fe/MWCNT) hybrid materials characterization: thermogravimetric analysis as a powerful characterization technique

Manuela Alzate[1] · Oscar Gamba[1] · Carlos Daza[2] · Alexander Santamaria[1] · Jaime Gallego[1,3,4]

Abstract

Nanomaterials and nanocomposites have gained relevance in science and technology due to their excellent properties. Therefore, the characterization of these materials is important. Thermogravimetric analysis is a powerful technique for the characterization of iron-carbon nanotubes (Fe/MWCNT) as hybrid nanomaterials, which may be prepared by impregnation step (alkaline or microwave-assisted precipitation). High-resolution transmission electron microscopy (HR-TEM), X-ray diffraction (XRD and in situ XRD), X-ray photoelectron spectroscopy (XPS), and thermogravimetric analysis (TGA) were the instrumental techniques used to characterize these hybrid materials. Through TGA, it was possible to determine the quantity of effective impregnated iron on the MWCNT. Further, in a TGA, nitrogen atmosphere reveals a thermal event reflecting the iron reduction by C from MWCNT and the shape of the signal reflects the dispersion and size of the iron particles on the surface. This thermal event is related to the particle sizes and chemical nature of iron oxides present. Thermal events from TGA may be correlated with the results obtained from XRD, XPS, and HR-TEM. The presence of smaller and well-distributed iron nanoparticles impacts the shape of the reducing event in the TGA. The reduction temperature as observed in TGA curves is related to the nature of metal compounds present, such as nitrates or oxides. These results suggest that TGA can be used as a rapid and economical technique for the evaluation of different Fe/MWCNT hybrid material properties. These results may facilitate the estimation of the structural and chemical nature of the Fe/MWCNT nanohybrid materials and permit the projections of potential applications.

Keywords Fe/MWCNT nanohybrid systems · TG analysis · Nanomaterials characterization

✉ Jaime Gallego
  Jaime.Gallego-Marin@phys.chemie.uni-giessen.de

1 Química de Recursos Energéticos y Medio Ambiente-QUIREMA., Instituto de Química, Universidad de Antioquia, Medellín, Colombia

2 Estado Sólido y Catálisis Ambiental, Departamento de Química, Facultad de Ciencias, Universidad Nacional de Colombia, Bogotá, D.C., Colombia

3 Center for Materials Research, Justus Liebig University, Heinrich-Buff-Ring 17, 35392 Giessen, Germany

4 Present Address: Institute of Physical Chemistry, Justus Liebig University, Heinrich-Buff-Ring 17, 35392 Giessen, Germany

Introduction

Thermogravimetric analysis has been used in the study of various materials. Among the applications of the technique, the study of oxidative and thermal stability of polymeric materials has been the most prominent [1], the characterization of energy sources such as biomass and petroleum [2, 3], as well as the analysis of nano-compounds has also been facilitated by thermogravimetry [4].

These analyses have extended to the characterization of nanohybrid systems of various metals supported on carbon nanostructures. The analyses have permitted the evaluation, among other characteristics of different oxide-reduction processes that occur in these systems [5]. The effect of parameters such as particle size on the various thermal processes presented by these materials [6], oxidation resistance [7] and the decomposition of the precursors used in the synthesis may be evaluated using this technique [8]. Nevertheless,

the use of the thermogravimetric analysis for the determination of chemical species in a nanohybrid system has not been explored. The availability of TGA methods to do this would be extremely useful to laboratories without access to robust equipment facilities such as X-ray diffraction and photoelectronic X-ray spectroscopy.

The interest in these nanohybrid systems has been based on their potential uses as catalytic systems [9, 10] and for their particular electromagnetic properties. On the other hand, it has been shown that the components of these nanohybrid systems may display cooperative effects that significantly improve their physicochemical properties. These properties have projected these materials with great potential for being used in various technologies such as the generation of biosensors, in the controlled release of medicaments, in antibacterial formulations and others [11]. Several characterization techniques have been used in the identification of the phases and the electronic configuration of the metals supported on carbon nanotubes. Prominent among these have been X-ray diffraction [11–13], XPS [8–14], and Mossbauer spectroscopy [15]. The use of thermogravimetric analyses as a powerful technique for hybrid nanomaterials Fe/MWCNT characterization has been demonstrated. Conclusions are supported by evidence collected using techniques such as TEM, XRD, and XPS.

Experimental

Carbon nanotubes synthesis and its acid functionalization

Multiwalled carbon nanotubes were obtained through an ethanol decomposition process at 900 °C in the presence of perovskite-like oxide ($LaFeO_3$) as catalytic precursor, as reported in a previous work [16]. The catalyst was placed into a horizontal reactor; the temperature was raised at 10 °C min^{-1} under N_2 atmosphere up to 900 °C and kept constant for 4 h. The obtained MWCNT were treated with a mixture of HNO_3 and H_2SO_4 (65% and 96 mass%, respectively, from Merck Chem, Germany) at a volumetric ratio of 3/1, for 15 min at 130 °C using a Milestone MicroSYNTH SK-10 microwave oven at an applied power of 500 W. The acid-treated product was filtered using a 0.45 µm cellulose filter (Whatman, United Kingdom), washed with distilled water and dried overnight at 100 °C. The filtered product consists of functionalized carbon nanotubes [17].

Iron supported on the functionalized MWCNT

Two different precipitation process were used to support the iron on the functionalized MWCNT, (a) the alkaline precipitation method and (b) the microwave-assisted polyol synthesis.

Alkaline precipitation methodology

For this methodology, 500 mg of functionalized MWCNT was dispersed into 50 mL of a 0.0016 M of iron nitrate aqueous solution ($Fe(NO_3)_3 \cdot 9H_2O$, Merck Chem, Germany). The concentration was adjusted so that the nominal Fe loading on MWCNT was around 10% by mass. The dispersion obtained was adjusted to pH 9.5 by dropwise addition of a 2.5% by mass of NH_3 solution under constant stirring for 30 min. The sample was filtered and washed with deionized water and dried overnight at 100 °C.

Microwave-assisted polyol synthesis

Usually, this synthesis method uses ethylene glycol, ($C_2H_6O_2$), as a solvent due to both: (1) its strong dipole moment that favors the absorption of microwave radiation and (2) it acts as a reducing agent for iron nanoparticles [18, 19]. For this method, 41.6 mg of functionalized MWCNT was dispersed into 20 mL of a 0.0041 M iron nitrate-ethylene glycol solution using an ultrasound water bath for 10 min. The reagents used for Fe solution preparation were supplied by Merk Chem, Germany and the nominal iron content on MWCNT was adjusted to be around 10% by mass. The mixture was heated at 200 °C for 15 min using a Milestone MicroSYNTH SK-10 microwave oven (high pressure segmented rotor) operated at 500 W. The sample was collected by filtration at reduced pressure, washed several times with distilled water and dried overnight at 100 °C. The samples obtained by the two methods were labeled as Fe AK (alkaline) and Fe MW (Microwave), respectively.

Physicochemical characterization

Thermogravimetric analysis: TGA

To follow the reactivity of the raw iron nanoparticles on MWCNT and their reactions, some TGA experiments were carried out in a TA-Instruments Q500 thermogravimetry analyzer equipment. For this experiment, 10 mg of Fe/MWCNT was placed inside the TGA furnace under a constant N_2 flow of 100 mL min^{-1} and a heating rate of 10 °C min^{-1} up to 950 °C. At 950 °C, the N_2 atmosphere was switched by air keeping the flow rate constant at 100 mL min^{-1} during 15 min to allow the oxidation of the MWCNT to CO_2 and the iron compounds to Fe_2O_3.

High-resolution transmission electron microscopy: HR-TEM

Morphology details and sizes of iron nanoparticles of the hybrid nanomaterial were determined by high-resolution transmission electron microscopy (HR-TEM) using a JEOL 2110 UHR instrument, at 200 kV accelerating voltage. The powder material was suspended in ethanol by sonication and a drop of the dispersion was deposited on a TEM copper lacey carbon grid and dried by natural evaporation.

Conventional and in situ X-ray diffraction analysis (XRD)

For conventional XRD analysis, diffraction patterns of the samples were recorded in a 2θ range between $10°$ and $90°$ using an XPert PANalytical Empyrian instrument equipped with a platform for reflection or transmission measurements and a Cu anode $K\alpha1 = 1.5406$ Å. In situ XRD experiments were conducted in a Panalytical X´PERT PRO MPD diffractometer with Cu $K_{\alpha1} = 1.5406$ Å, operated at 45 kV and 40 mA. The diffraction patterns were recorded in a 2θ interval from $4°$ to $70°$ with a scanning step size of $0.013°$ and 59 s per step. The sample was first degasified in argon (Linde, United Kingdom. 5.0 of purity) during 20 min at $50\ °C$ at a flow of $20\ mL\ min^{-1}$, then, under the same argon atmosphere, the temperature was increased at heating rate of $10\ °C\ min^{-1}$ from 50 to $900\ °C$ followed by an isothermal step at $900\ °C$ for 30 min. Diffraction patterns were recorded every $50\ °C$.

X-ray photoelectron spectroscopy

Hybrid nanomaterial was characterized by X-ray photoelectron spectroscopy (XPS) using a Specs X-ray photoelectronic spectrometer (NAP-XPS) equipped with a monochromatic source of $Al-K_{\alpha}$ (1486.7 eV, 13 kV, 100 W) along with a PHOIBOS 150-1D-DLD analyzer. Energies of 100 eV (1 eV $step^{-1}$) during three measurement cycles and 20 eV (0.1 eV $step^{-1}$) in ten measurement cycles were used for survey and high-resolution spectra, respectively. The system is equipped with a in situ gas-pressure cell which could be operated until 25 mbar, while the outside of the cell is at UHV conditions (Base pressure of the system was 1.3×10^{-10} mbar). The cell includes a filament behind the sample using the electron beam methods or radiative heating to heat the sample. Three experiments were carried out, each of them under the scanner conditions mentioned above. First, a spectrum was taken at room temperature under UHV conditions. Afterward, the sample was exposed to 2 mbar of Argon at $500\ °C$. When the temperature was achieved, a spectrum was taken. Finally, the sample is cooling down and annealing at $500\ °C$ under UHV conditions. Once the temperature was achieved, a spectrum was taken.

N_2-physisorption

Nitrogen adsorption–desorption isotherms were obtained in a Micromeritics ASAP 2020 instrument. Before analysis, the samples were degassed at $250\ °C$ for 12 h. The specific surface area was determined using the BET method, and pore volume and pore size distribution were determined using the BJH method.

Results and discussion

In previous works, it was shown that the thermocatalytic decomposition of ethanol is an efficient process to produce large quantities of carbonaceous materials such as carbon nanotubes and hydrogen [16]. These MWCNT have been characterized, modified, and used for different purposes, such as titanium reinforcement, electrochemical sensors, catalyst support, among others [20–24], showing remarkable performances. Methodologies such as alkaline precipitation and microwave-assisted polyol have been reported to be used to support transition element nanoparticles on the surface of multiwalled carbon nanotubes [15, 25–30], creating hybrid metal/MWCNT nanosystems that have been already tested as electrochemical sensors [24, 25]. This research focuses on the characterization of these nanohybrid systems by means of different instrumental techniques and the understanding of the thermal behavior in each stage of nanoparticle formation of nanoparticles allowing the interpretation of parameters associated to crystalline phases and particle diameter distribution according to the synthesis method. The obtained hybrid iron/MWCNTmaterials were characterized by thermogravimetric analysis in order to find some differences in their thermal behavior. In general, all samples showed three main thermal events under N_2 atmosphere, as shown in Fig. 1. The first thermal event at $310\ °C$ corresponds to the oxygenated functional groups decomposition which were previously formed during the acid treatment (Fig. 1a, Eq. 1). [27, 31]. Chemical compounds such as carboxylic acids, ketons, aldehydes, alcohols have been reported for this type of acid functionalization process. On the other hand, the second event occurred at around $860\ °C$ (Fig. 1b) corresponding to the in situ iron species reduction caused by the presence of carbon from MWCNT following the process described in Eq. 2.

$$C_{CNT} - COOH \xrightarrow{heat\ under\ inert\ atmosphere} CO_x + H_2O + C_{CNT} \tag{1}$$

$$Fe_zO_y + \frac{y}{x}C_{CNT} \xrightarrow{heat\ under\ inert\ atmosphere} \frac{1}{x}CO_y + zFe^0 \tag{2}$$
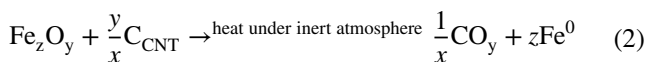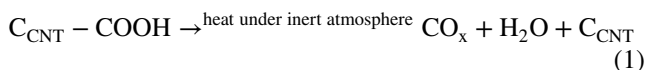
where CO_y could be either CO or CO_2.
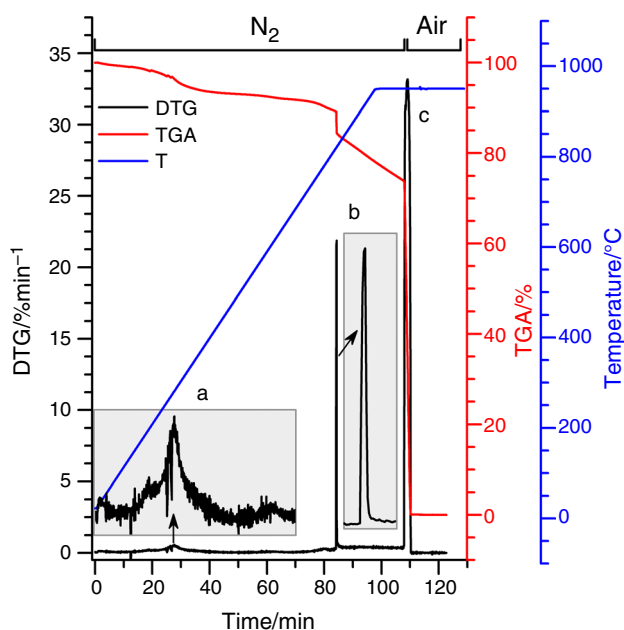
Fig. 1 Thermogravimetric analysis for the Fe/MWCNT nanohybrid system obtained by the microwave-assisted polyol process methodology. The thermal events are presented: **a** decomposition of the carbon nanotubes functional groups, **b** reduction of iron species in a nitrogen atmosphere and **c** oxidation of carbon and iron nanotubes in air atmosphere

Subsequently, at 900 °C, when the N_2 atmosphere was switched by air, the oxidation event occurred (Fig. 1c and Eq. 3). Then, the yellow–brown residue obtained corresponds to hematite (Fe_2O_3), the most stable iron oxide phase at those conditions [32, 33]. As showed in previous reports, during this acidic functionalization, a high quantity of superficial functional groups is formed over the MWCNT, and at the same time, a purification takes place regarding amorphous materials and catalyst residues. Figure S1 shows (see the supplementary information) a typical TGA/DTG for those MWCNT after a functionalization/purification process [5, 17, 34, 35].

$$C_{CNT} + \frac{5}{2}O_{2(air)} + 2Fe^0 \rightarrow CO_2 + Fe_2O_3 \qquad (3)$$
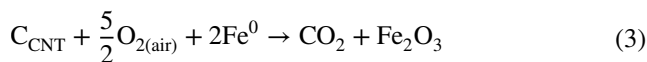
The differences in the reduction events, under N_2, for the nanohybrid materials synthesized by the two methodologies are shown in Fig. 2. Table 1 also shows the maximum temperatures and the full width at a half maximum of the iron reduction events observed. It is possible to see how the preparation method has a strong influence on the thermal behavior of the M@MWCNT nanohybrid systems, indicating structural and chemical changes in the phases obtained. For instance, the FeAK sample (Fig. 2a) presented larger full width at a half maximum possibly due to larger particle size or a mixture of crystalline phases as may also be reflected
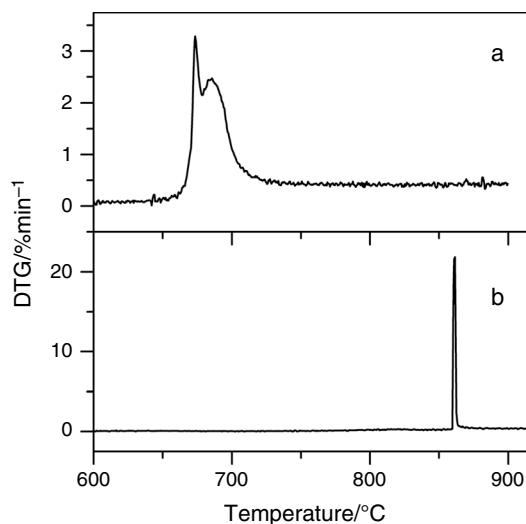
Fig. 2 DTG profiles showing reduction events in N_2 atmosphere for nanohybrid systems **a** Fe AK y **b** Fe MW

by the existence of two nearby peaks. The narrowing in the event shown in Fig. 2b could refer to a higher speed in the reduction reaction of the nanoparticle due smaller particle sizes [36, 37].

To determine the crystalline phases present in the nanohybrid systems, X-ray diffraction experiments were performed at room temperature: Crystalline phases of iron oxide species corresponding to hematite or magnetite (Fig. 3b) were found to be negligible on the nanohybrid material mainly due to high degree of carbon graphitization of the nanotubes. Additionally, the samples have not yet undergone heat treatment, so they are expected to be poorly crystalline and in the nanometric size range [38]. This figure also displays the diffraction planes of carbon nanotubes that are similar to those found for a graphite-like systems with some changes in the signal shifts due to MWCNT curvature (ICSD 98-005-3781).

To find more information about the thermal behavior of nanohybrid systems and the structuring of nanoparticles, characterization was performed using in situ XRD under N2 atmosphere. In Fig. 4a, contour map with three axes is presented. The x-axis shows the diffraction angle, the y-axis shows the temperature increase during the XRD analysis,

Table 1 Summary of Fe percentual, reduction temperature, and full width at half maximum of nanoparticles obtained by TG analysis for the three synthesis methods

Sample	Mass fraction of Fe in the hybrid material/%	Temperature reduction/°C	Full width at half maximum/°C
Fe AK	9.75	670	26.58
Fe MW	9.58	860	2.03
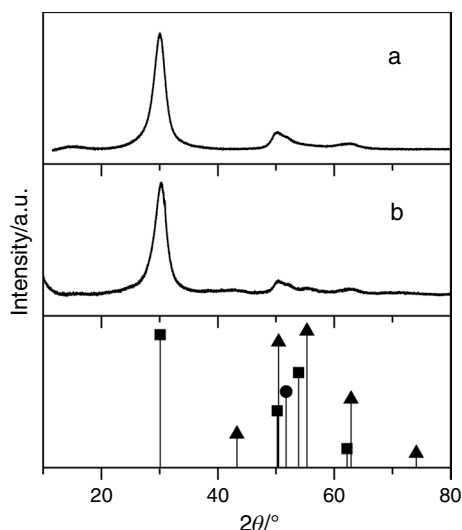
Fig. 3 X-ray diffraction patterns at room temperature for **a** functionalized carbon nanotubes and **b** Fe MW nanohybrid system with standard diffraction patterns for carbon nanotubes (square), magnetite (triangle) and iron (circle)

and the z-axis represents the intensity of the signal. The intensity scale bar indicates that the intensity tends to zero when is black and increases when is white bright. It has been reported that increasing the temperature around 300 °C [5] favors the crystallization of magnetite (Fe_3O_4), via a partial reduction of Fe^{3+} oxide, according to Eq. 4, and as shown in Fig. 4.

$$3Fe_2^{3+}O_3^{2-} + \frac{1}{x}C_{CNT} \rightarrow 2Fe_1^{2+}Fe_2^{3+}O_4^{2-} + \frac{1}{x}CO_x \qquad (4)$$
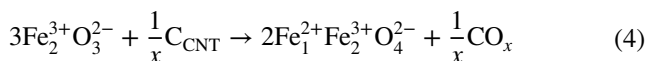
For larger iron particle sizes with an exposed surface and that do not have direct contact with carbon nanotubes, the effect of temperature produced a change from Fe(III) to Fe(II), while the smaller particles, being in better contact with the carbon nanotube (reducing agent), caused the change from Fe(III) to Fe(0) in a single step.

During the reduction process, the samples presented different crystalline phases. For example, the reduction event at 700 °C in the Fe AK sample was associated with the formation of FeO (ICSD 98-006-7198) and Fe^0 (ICSD 98-063-1730) crystalline phases. This explains the doublet observed in the DTG profile of Fig. 2a, confirming the partial reductions of the iron nanoparticle. The reduction process for the Fe AK system is illustrated in Fig. 5. On the exposed surface of larger iron nanoparticles that are not in contact with the carbon nanotube, the effect of temperature produced a reduction step from Fe(III) to Fe(II), while the smallest ones being in intimate contact with the carbon nanotubes caused the reduction in Fe(III) to Fe(0) in a one-step process.

On the other hand, when the Fe MW sample reached a temperature of 860 °C, a single and homogeneous reduction event corresponding to the metallic iron phase formation was seen. This indicates that the microwave-assisted synthesis method generates smaller and better distributed particle sizes than the Fe AK sample [11, 39–43].

To recap, the thermal reduction events for the Fe AK sample involve the successive transformation of different iron oxides to metallic iron, as illustrated from Eqs. 5 to 8, while the thermal event for the Fe MW sample corresponds to the crystallization-reduction process of the magnetic iron oxide (Fe_3O_4) to produce metallic iron, according to Eq. 7.
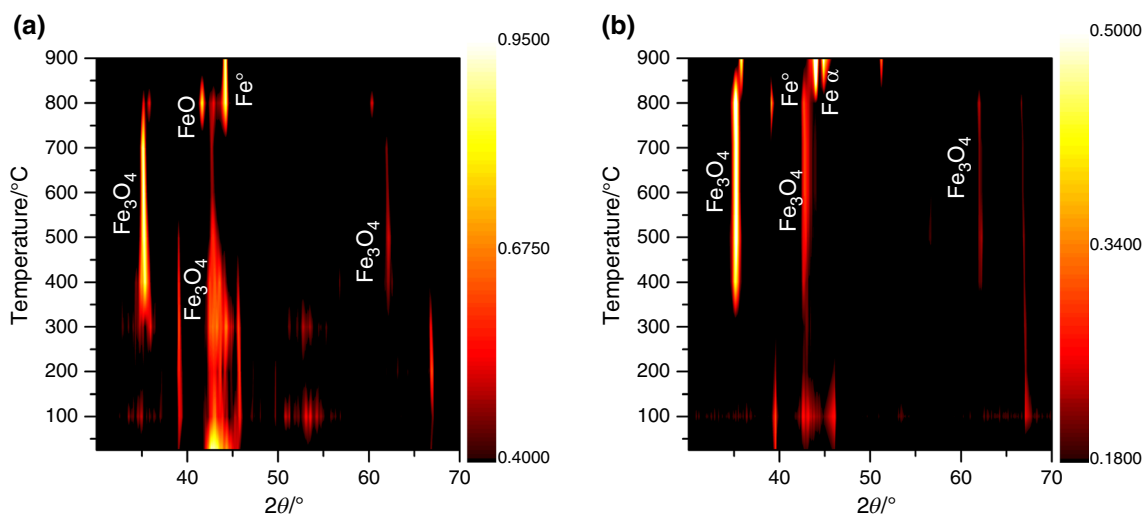
Fig. 4 In situ X-ray diffraction (contour map) in inert atmosphere (Ar) for **a** Fe AK and **b** Fe MW. From room temperature to 900 °C. Intensity scale bar, as darkest the intensity tend to cero, and as lightest, the intensity increases

Fig. 5 Illustration of the successive reduction steps of the nanoparticle impregnated in the carbon nanotube by alkaline precipitation method

$$3Fe_2O_3 + \frac{1}{x}C_{CNT} \rightarrow \frac{1}{x}CO_x + 2Fe_3O_4 \quad (5)$$

$$Fe_3O_4 + \frac{1}{x}C_{CNT} \rightarrow \frac{1}{x}CO_x + 3FeO \quad (6)$$

$$FeO + \frac{1}{x}C_{CNT} \rightarrow \frac{1}{x}CO_x + Fe° \quad (7)$$

$$Fe_3O_4 + \frac{4}{x}C_{CNT} \rightarrow \frac{4}{x}CO_x + 3Fe° \quad (8)$$
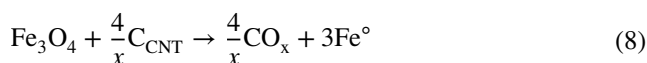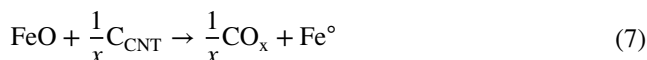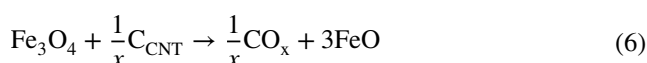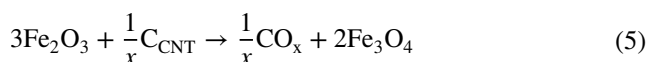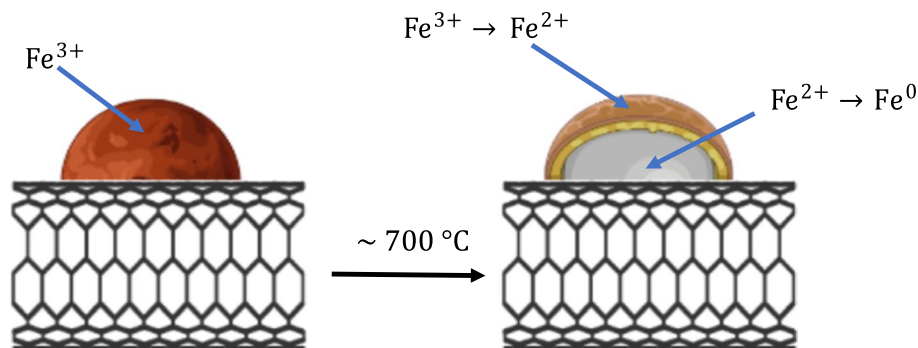
In a thermodynamic study reported in [44], it was found that in nanosystems, as the particle size of the reactants decreases, the Gibbs free energy becomes more negative, making in the metal oxide formation of more favorable, while the reverse reaction (reduction) will require higher temperature. Therefore, the 170 °C difference observed in DTG between the reduction temperature of the iron oxides obtained by microwave-assisted and alkaline precipitation methods (Table 1) was possibly due to differences in particle sizes, being smaller for Fe MW sample. This result demonstrates that thermogravimetric analysis is a powerful tool for predicting the behavior of nanosystems not only through their particle size and its correlation with their thermodynamic properties but also their crystallinity through the homogeneity and shape of DTG curves.

To confirm the iron nanoparticle sizes and their distribution on carbon nanotubes, transmission electron microscopy was used. For the Fe AK sample, after measuring 43 particles, it averaged an iron particle size of 35.0 nm with a standard deviation of 14.0 nm, indicating that the alkaline synthesis method does not lead to the formation of uniform size nanoparticles on carbon nanotubes, as seen in Fig. 6a, b. In contrast, the Fe MW nanohybrid system, counting 44 particles, gave a mean iron particle size of 19.0 nm with a standard deviation of 6.0 nm, confirming that the microwave-assisted method produces smaller and more homogeneous nanoparticles than other chemical methods, as seen in Fig. 6d.

The nature of the iron species in the nanohybrid systems and its behavior under reducing conditions was investigated using XPS analysis. XPS measurements were conducted under different pressure and temperature conditions in the Fe 2p region.

The Fe 2p3/2 peak appears narrower, more intense, and larger in area than that observed for the Fe 2p1/2 peak.

Figure 7a shows the XPS peaks corresponding to the Fe $2p_{3/2}$ and Fe $2p_{1/2}$ states of iron in the FeAK sample when the XPS analysis was performed at room temperature and ultra-high-vacuum (UHV) conditions without further treatment. The Fe $2p_{3/2}$ peak appears narrower, more intense and with larger area than that observed for the Fe $2p_{1/2}$ peak. This observation agrees with the expected spin–orbit (j-j) coupling [45], where the Fe $2p_{3/2}$ peak has four-state degeneracy, while the Fe $2p_{1/2}$ has only two [45, 46]. The Fe 2p3/2 and Fe 2p1/2 binding energies are 711.5 eV and 725. 1 eV, respectively, the spectrum also shows a signal at 719.2 eV which does not overlap with the previous ones. This signal has been associated with a satellite peak of Fe $2p_{3/2}$. The overall spectrum with the presence of this satellite resembles the spectrum obtained for α-Fe$_2$O$_3$ (hematite) which correspond to a material with an iron oxidation state of 3 + [45].

Figure 7b shows the spectrum taken at 500 °C under 2 mbar of Argon. The Fe $2p_{3/2}$ and Fe $2p_{1/2}$ peak positions were 710.3 eV and 723.4 eV, respectively. The spectrum also shows a shoulder at the high-energy site of the Fe $2p_{3/2}$ peak (716.4 eV) associated with the satellite peak of that iron state. Although this peak appears at lower energies values compared to the previous satellite (Fig. 7a), the signal displacement could be associated with the reduction process from Fe(III) to Fe(II) in the nanohybrid materials. Similar spectra have reported in [45] indicating the presence of Fe(II) in 2FeO·SiO$_2$ samples [45].

On the other hand, when the sample was annealed at 500 °C under UHV conditions, the spectrum showed a signal at 706.9 eV corresponding to the Fe 2p peak. This lower binding energy could indicate the reduction from
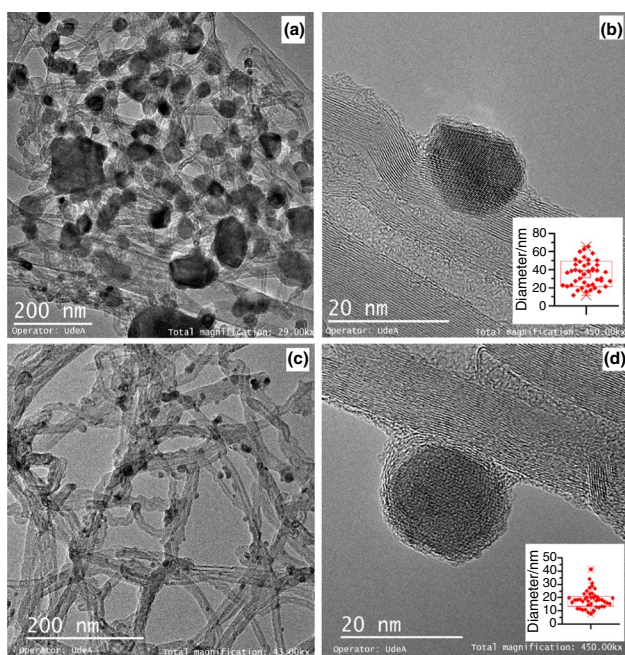
Fig. 6 TEM images for the Fe AK nanohybrid system (**a**, **b**) and the Fe MW nanohybrid system (**c**, **d**). In the insets, the box-plot for the particle size distributions of both samples was introduced

Fe(II) to Fe(0), see Fig. 7c. The XPS spectra allowed us to conclude that the Fe species on MWCNT (Fe/MWCNT hybrid material) can be partially or completed reduced depending on the heating temperature due to the reducing effect of carbon [47, 48].

The characterization results agree with each other. From TGA-DTG analysis, different thermal events could be found, including the iron reduction by reacting with carbon from MWCNT. This particular thermal event was different between preparation methods suggesting differences in the chemical and structural properties of the samples. In situ XRD analysis also indicated that the transformation steps from amorphous iron to metallic iron were dependent on sample preparation. Finally, XPS showed that the prepared Fe/MWCNT nanohybrid systems contain iron with a mixture of oxidation states (3+ and 2+), which can be reduced to metallic iron in the presence of carbon by increasing the temperature under inert atmosphere.

Finally, these hybrid materials are conceived for several applications between them as catalysts and adsorbents, where the textural properties are relevant. N2 physisorption was done to determine the surface area and porosity. As it is shown in Figure S2, these iron impregnation methodologies, and iron itself, are not significantly changing these properties. For the surface area, an increasing was found, from 142 to 171 $m^2 g^{-1}$ and 181 $m^2 g^{-1}$, starting from the raw functionalized MWCNT, Fe MW and Fe AK, respectively, iron hybrid samples. This change can be related to a reorganization of the
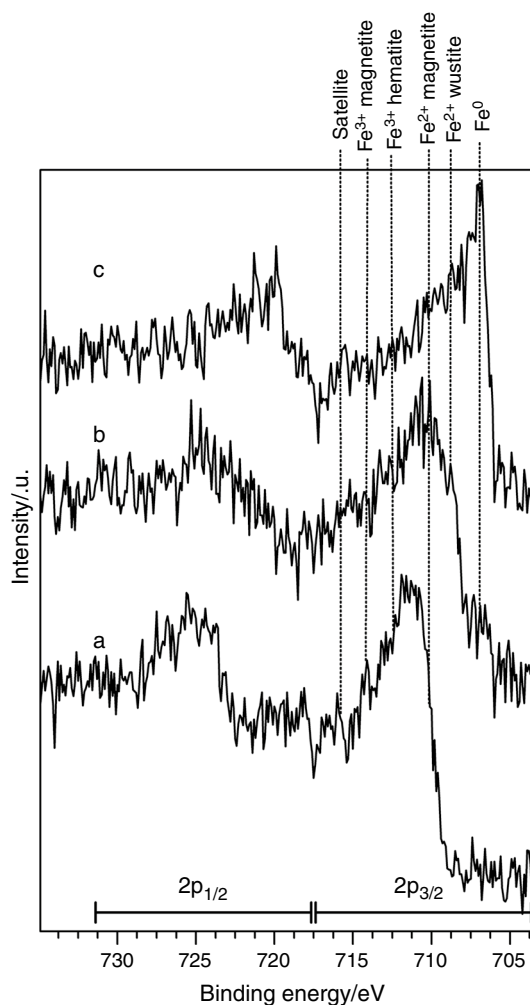
Fig. 7 In situ XPS spectra for Fe AK sample at different conditions. **a** Room temperature under UHV conditions **b** 500 °C under 2 mbar of argon. **c** 500 °C under UHV conditions.

nanotubes in their agglomerates promoted for the solvents, agitation, and all the operation during iron impregnation. Looking at the porosity, it is possible to see that the three materials have the same mesoporous structure with two general type of pores. First centered at 2.4 nm, can be related to the inner cavity of the nanotubes and open at the ends, second centered at 22 nm, and wider can be related to the porosity formed for the nanotube folding or agglomerating with others nanotubes [49, 50].

Conclusions

It was found that the synthesis methods used in this study to prepare the Fe/MWCNT nanohybrid systems generate some changes in the crystalline phases and particle sizes of iron oxides species. The nanohybrid systems synthesized by microwaves (Fe MW) produced particles with smaller and

more homogeneous sizes compared to nanohybrid systems synthesized by the alkaline method (Fe AK).

By impregnating nanoparticles on the nanotubes functionalized by the microwave-assisted synthesis method, particles with smaller sizes and good homogeneity were generated, this is due to microwave heating is more homogeneous and the use of solvents such as ethylene glycol, which is also. It is an excellent reducing agent, promotes greater control over the oxidation states and the size of the nanoparticles supported on the carbon nanotubes, which was evidenced in the transmission electron micrograph.

The use of the different instrumental characterization techniques, and the correlation of the results, showed that thermogravimetric analysis (TGA) is a fast, inexpensive, and versatile technique to estimate the nature of the nanoparticles deposited on carbon nanotubes and their quantity. Furthermore, these results open a field of research in instrumental analysis since this technique allows characterizing materials at a structural level like distribution and particle size.

In the synthesis of Fe/MWCNT nanohybrid systems, it was found that the methodologies used generate changes in the crystalline phases, sizes of the nanoparticles and their homogeneity and do not change significantly the textural properties comparing to the original functionalized MWCNT.

Declarations

Conflict of interest The authors have no conflicts of interest to declare that are relevant to the content of this article.

References

1. Badia JD, Martinez-Felipe A, Santonja-Blasco L, Ribes-Greus A. Thermal and thermo-oxidative stability of reprocessed poly(ethylene terephthalate). J Anal Appl Pyrolysis. 2013;99:191–202.
2. Saldarriaga JF, Aguado R, Pablos A, Amutio M, Olazar M, Bilbao J. Fast characterization of biomass fuels by thermogravimetric analysis (TGA). Fuel. 2015;140:744–51.
3. Kök MV, Varfolomeev MA, Nurgaliev DK. Crude oil characterization using TGA-DTA, TGA-FTIR and TGA-MS techniques. J Pet Sci Eng. 2017;154:537–42.
4. Chipara M, Lozano K, Hernandez A, Chipara M. TGA analysis of polypropylene-carbon nanofibers composites. Polym Degrad Stab. 2008;93:871–6.
5. Gallego J, Tapia J, Vargas M, Santamaria A, Orozco J, Lopez D. Synthesis of graphene-coated carbon nanotubes-supported metal nanoparticles as multifunctional hybrid materials. Carbon N Y. 2017;111:393–401.
6. Lorençon E, Lacerda RG, Ladeira LO, Resende RR, Ferlauto AS, Schuchardt U, et al. Thermal behavior of carbon nanotubes decorated with gold nanoparticles. J Therm Anal Calorim. 2011;105:953–9.
7. Liu Q, Ren W, Chen Z-G, Liu B, Yu B, Li F, et al. Direct synthesis of carbon nanotubes decorated with size-controllable Fe nanoparticles encapsulated by graphitic layers. Carbon N Y. 2008;46:1417–23.
8. Karousis N, Tsotsou G-E, Evangelista F, Rudolf P, Ragoussis N, Tagmatarchis N. Carbon nanotubes decorated with palladium nanoparticles: synthesis, characterization, and catalytic activity. J Phys Chem C. 2008;112:13463–9.
9. Wildgoose GG, Banks CE, Compton RG. Metal nanoparticles and related materials supported on carbon nanotubes: methods and applications. Small. 2006;2:182–93.
10. Gao C, He H. Synthesis of Fe3O4/Pt nanoparticles decorated carbon nanotubes and their use as magnetically recyclable catalysts. In: Huang J, editor. J nanomater, vol. 2011. Hindawi Publishing Corporation; 2011. p. 193510.
11. Chen WX, Lee JY, Liu Z. Preparation of Pt and PtRu nanoparticles supported on carbon nanotubes by microwave-assisted heating polyol process. Mater Lett. 2004;58:3166–9.
12. Rajarao R, Jayanna RP, Sahajwalla V, Bhat BR. Greenapproach to decorate multi-walled carbon nanotubes by metal/metal oxide nanoparticles. Procedia Mater Sci. 2014;5:69–75.
13. Fan XJ, Li X. Preparation and magnetic properties of multiwalled carbon nanotubes decorated by Fe3O4 nanoparticles. Xinxing Tan Cailiao/New Carbon Mater. 2012;27:111–6.
14. Bittencourt C, Felten A, Ghijsen J, Pireaux JJ, Drube W, Erni R, et al. Decorating carbon nanotubes with nickel nanoparticles. Chem Phys Lett. 2007;436:368–72.
15. Huiqun C, Meifang Z, Yaogang L. Decoration of carbon nanotubes with iron oxide. J Solid State Chem. 2006;179:1208–13.
16. Gallego J, Sierra G, Mondragon F, Barrault J, Batiot-Dupeyrat C. Synthesis of MWCNTs and hydrogen from ethanol catalytic decomposition over a Ni/La2O3 catalyst produced by the reduction of LaNiO3. Appl Catal A Gen. 2011;397:73–81.

17. Blandón-Naranjo L, Della Pelle F, Vázquez MV, Gallego J, Santamaría A, Alzate-Tobón M, et al. Electrochemical behaviour of microwave-assisted oxidized MWCNTs based disposable electrodes: proposal of a NADH electrochemical sensor. Electroanalysis. 2018;30:509–16.
18. Komarneni S, Katsuki H, Li D, Bhalla AS. Microwave-polyol process for metal nanophases. J Phys Condens Matter. 2004;16:S1305.
19. Komarneni S, Li D, Newalkar B, Katsuki H, Bhalla AS. Microwave: Polyol process for Pt and Ag nanoparticles. Langmuir. 2002;18:5959–62.
20. Zhang M, Smith A, Gorski W. Carbon nanotube−chitosan system for electrochemical sensing based on dehydrogenase enzymes. Anal Chem. 2004;76:5045–50.
21. De Volder MFL, Tawfick SH, Baughman RH, Hart AJ. Carbon nanotubes: present and future commercial applications. Science. 2013;339:535–9.
22. Ahammad AJS, Lee J-J, Rahman MA. Electrochemical sensors based on carbon nanotubes. Sensors. 2009;9:2289–319.
23. Bianco A, Kostarelos K, Prato M. Applications of carbon nanotubes in drug delivery. Curr Opin Chem Biol. 2005;9:674–9.
24. Sun L, Wang X, Wang Y, Zhang Q. Roles of carbon nanotubes in novel energy storage devices. Carbon. 2017;122:462–74.
25. Ghaemi F, Ali M, Yunus R, Othman RN. Synthesis of carbon nanomaterials using catalytic chemical vapor deposition technique. Synth Technol Appl Carbon Nanomater. 2018;2019:1–27.
26. Tran TQN, Das G, Yoon HH. Nickel-metal organic framework/MWCNT composite electrode for non-enzymatic urea detection. Sens Actuat B Chem. 2017;243:78–83.
27. Jiang L, Gao L. Carbon nanotubes−magnetite nanocomposites from solvothermal processes: formation, characterization, and enhanced electrical properties. Chem Mater. 2003;15:2848–53.
28. Mai YJ, Tu JP, Gu CD, Wang XL. Graphene anchored with nickel nanoparticles as a high-performance anode material for lithium ion batteries. J Power Sources. 2012;209:1–6.
29. Zhang W-D, Xu B, Jiang L-C. Functional hybrid materials based on carbon nanotubes and metal oxides. J Mater Chem. 2010;20:6383.
30. Zhang R, He S, Lu Y, Chen W. Fe Co, N-functionalized carbon nanotubes in situ grown on 3D porous N-doped carbon foams as a noble metal-free catalyst for oxygen reduction. J Mater Chem A. 2015;3:3559–67.
31. Soto D, Alzate M, Gallego J, Orozco J. Electroanalysis of an iron@graphene-carbon nanotube hybrid material. Electroanalysis. 2018;30:1521–8.
32. Kuzmany H, Kukovecz A, Simon F, Holzweber M, Kramberger C, Pichler T. Functionalization of carbon nanotubes. Synth Met. 2004;141:113–22.
33. Bonalume BCF, Lebrão GW, Rossi JL. Microwave assist functionalization of multi walled carbon nanotubes. ECCM 2012 - Compos Venice, Proc 15th Eur Conf Compos Mater. 2012. p. 24–8.
34. Gallego J, Batiot-Dupeyat C, Mondragón F. Activation energies and structural changes in carbon nanotubes during different acid treatments. J Therm Anal Calorim. 2013;114:597–602.
35. Avilés F, Cauich-Rodríguez JV, Moo-Tah L, May-Pat A, Vargas-Coronado R. Evaluation of mild acid oxidation treatments for MWCNT functionalization. Carbon N Y. 2009;47:2970–5.
36. Signorini L, Pasquini L, Savini L, Carboni R, Boscherini F, Bonetti E, et al. Size-dependent oxidation in iron/iron oxide core-shell nanoparticles. Phys Rev B Condens Matter Mater Phys. 2003;68:1–8.
37. Nurmi JT, Tratnyek PG, Sarathy V, Baer DR, Amonette JE, Pecher K, et al. Characterization and properties of metallic iron nanoparticles: spectroscopy, electrochemistry, and kinetics. Environ Sci Technol. 2005;39:1221–30.
38. de Resende VG, Peigney A, De Grave E, Laurent C. In situ high-temperature Mössbauer spectroscopic study of carbon nanotube–Fe–Al2O3 nanocomposite powder. Thermochim Acta. 2009;494:86–93.
39. Wang Y, Iqbal Z, Mitra S. Microwave-induced rapid chemical functionalization of single-walled carbon nanotubes. Carbon N Y. 2005;43:1015–20.
40. Sun Y-P, Fu K, Lin Y, Huang W. Functionalized carbon nanotubes: properties and applications. Acc Chem Res. 2002;35:1096–104.
41. Datsyuk V, Kalyva M, Papagelis K, Parthenios J, Tasis D, Siokou A, et al. Chemical oxidation of multiwalled carbon nanotubes. Carbon N Y. 2008;46:833–40.
42. Przepiera K, Przepiera A. Kinetics of thermal transformations of precipitated magnetite and goethite. J Therm Anal Calorim. 2001;65:497–503.
43. Sorescu M, Xu T. Particle size effects on the thermal behavior of hematite. J Therm Anal Calorim. 2012;107:463–9.
44. Du J, Zhao R, Xue Y. Effects of sizes of nano-copper oxide on the equilibrium constant and thermodynamic properties for the reaction in nanosystem. J Chem Thermodyn. 2012;45:48–52.
45. Yamashita T, Hayes P. Analysis of XPS spectra of Fe2+ and Fe3+ ions in oxide materials. Appl Surf Sci. 2008;254:2441–9.
46. Biesinger MC, Payne BP, Grosvenor AP, Lau LWM, Gerson AR, Smart RSC. Resolving surface chemical states in XPS analysis of first row transition metals, oxides and hydroxides: Cr, Mn, Fe. Co and Ni Appl Surf Sci. 2011;257:2717–30.
47. Xu Y. Carbon-covered magnetic nanomaterials and their application for the thermolysis of cancer cells. Int J Nanomed. 2010;5:167.
48. Lin TC, Seshadri G, Kelber JA. A consistent method for quantitative XPS peak analysis of thin oxide films on clean polycrystalline iron surfaces. Appl Surf Sci. 1997;119:83–92.
49. Yang C-M, Kaneko K, Yudasaka M, Iijima S. Effect of purification on pore structure of hipco single-walled carbon nanotube aggregates. Nano Lett. 2002;2:385–8.
50. Lee PL, Chiu YK, Sun YC, Ling YC. Synthesis of a hybrid material consisting of magnetic iron-oxide nanoparticles and carbon nanotubes as a gas adsorbent. Carbon. 2010;48:1397–404.